Conf-9010135--28

Environmentally Assisted Cracking In Light Water Reactors*

J. Y. Park, W. E. Ruther, T. F. Kassner, and W. J. Shack

Materials and Components Technology Division
Argonne National Laboratory
Argonne, Illinois 60439 USA

ANL/CP--70988

DE91 011167

December 1990

DISCLAIMER

Presented at the Eighteenth Water Reactor Safety Information Meeting, October 22-24, 1990, Rockville, MD.

*Work supported by the Office of Nuclear Regulatory Research, U. S. Nuclear Regulatory Commission.

Environmentally Assisted Cracking In Light Water Reactors

J. Y. Park, W. E. Ruther, T. F. Kassner, and W. J. Shack

Materials and Components Technology Division
Argonne National Laboratory
Argonne, Illinois 60439 USA

Abstract

Topics that have been investigated during this year include (1) SCC of A533-Gr B steel used in steam generator and reactor pressure vessels, (2) fatigue of Type 316NG SS, and (3) SCC of Type 347 and CF-3 cast duplex stainless steels in simulated BWR water. Crack-growth-rate (CGR) tests were performed on a composite A533-Gr B/Inconel-182 specimen in which the stress corrosion crack in the Inconel-182 weld metal penetrated and grew into the A533-Gr B steel. CGR tests were also conducted on conventional (unplated) and nickel- or gold-plated A533-Gr B specimens to provide insight into whether the nature of the surface layer on the low-alloy steel, either oxide corrosion products or a noble metal, influences the overall SCC process. CGR data on the A533-Gr B specimens were compared with the fatigue crack reference curves in the ASME Boiler and Pressure Vessel Code, Section XI, Appendix A. Fatigue tests were conducted on Type 316NG SS in air and simulated BWR water at low strain ranges and frequencies to better establish margins in the ASME Code Section III Fatigue Design Curves. CGR tests were also conducted on specimens of Type 347 SS with different heat-treatment conditions, and a specimen of CF-3 cast stainless steel with a ferrite content of 15.6%. The results were compared with previous data on another heat of Type 347 SS, which was very resistant to SCC, and a CF-3M steel with a ferrite content of 5%.

1 Introduction

Environmentally assisted cracking of piping and pressure vessels in light water reactors (LWRs) is an important concern as extended reactor lifetimes are envisaged. Intergranular stress corrosion cracking (SCC) of austenitic stainless steel (SS) piping in boiling water reactors (BWRs) has required research, inspection, and mitigation programs that have cost several billion dollars. More recently, cracks that have initiated in sensitized stainless steels have propagated into low-alloy ferritic steels in BWR pressure vessels, and extensive cracking has occurred in upper shell-to-transition cone girth welds in pressurized water reactor (PWR) steam generator vessels. Research during the past year focused on (1) SCC of ferritic pressure vessel steel, (2) fatigue of Type 316NG SS, and (3) SCC of alternative austenitic SS for BWR piping.

2 Summary of Research Progress

2.1 Stress Corrosion Cracking of Ferritic Steels

Plain carbon and low-alloy steels are used extensively as piping and pressure vessel materials in PWRs and BWRs. These steels include A106-Gr B and A333-Gr 6 for seamless pipe and A302-Gr B, A508-2, and A533-Gr B plate for pressure vessels. Although operating experience with these steels is better than with weld-sensitized austenitic SS, instances of cracking of ferritic steel components that comprise the reactor pressure boundary have occurred in the United States and abroad. Over the past 15 years, the corrosion fatigue properties of these steels in LWR primary system water chemistries have been studied extensively.[1-3] Much less information is available on the SCC of these materials.[4-8] Because it is clear that very high SCC growth rates can occur under some combinations of materials, loading, and environment, the objective of the current work is to better define the conditions that can produce SCC in these steels.

2.1.1 Experimental Methods

Fracture-mechanics crack-growth-rate (CGR) tests have been carried out on a heat of high sulfur (0.019 wt.%) A533-Gr B pressure vessel steel. The chemical composition is given in Table 1. In addition to conventional 1-T compact-tension specimens, specimens plated with either nickel or gold, together with a composite specimen of A533-Gr B/Inconel-182/Inconel-600 plated with nickel, were tested. The nickel-plated specimens were used to better simulate a clad ferritic steel vessel, where only the low-alloy steel at the crack surface is exposed to the environment. The surface films on the nickel and gold plated specimens will be very different from those on the unplated ferritic specimens. Electron transfer through the oxide film on the bulk surface of the ferritic steel is a potentially important rate-limiting process. Because virtually all of the existing data have been obtained on specimens without cladding, it is important to verify that those results were not unduly affected by the character of the surface film.

The conventional and plated specimens were tested in simulated BWR water with ≈200 ppb dissolved oxygen at 289°C under cyclic loading with a positive sawtooth wave form (12-s loading and 1-s unloading time) at 0.08 Hz, load ratios ($R = K_{min}/K_{max}$) of 0.25 to 0.95, and maximum stress intensities, K_{max}, of ≈21 to 60 MPa·m$^{1/2}$. The tests on the composite specimen were conducted in high-purity water with ≈200 ppb dissolved oxygen at an R value of 0.95, a frequency of 0.08 Hz for the positive sawtooth wave form, and K_{max} values of 28 to 102 MPa·m$^{1/2}$. Crack-length measurements were made by a DC potential drop technique in the conventional and plated specimens. Because no potential drop calibration was available for the composite specimen, crack length was measured by the compliance method.

Table 1. Chemical Composition (wt.%) of A533–Gr B Steel/Inconel–182 Weld Metal/Alloy–600 and A533–Gr B Compact Tension Specimens[a] for Crack Growth Tests

Material	C	P	S	Si	Fe	Cr	Ni	Mn	Mo	Ta/Nb	Ti
A533–Gr B[b]	0.22	0.011	0.019	0.22	Bal	0.12	0.69	1.45	0.53	–	–
In–182[c]	0.1	0.03	0.01	1.0	10.0	14.0	65.0	7.0	–	1.75	1.0
In–600	0.07	–	0.001	0.19	9.41	15.23	73.84	0.30	–	0.12	0.31

[a]Composite Alloy–600/In–182/A533–Gr B compact tension (1T) specimen was fabricated such that the low–alloy steel was in the T–L orientation according to the ASTM nomenclature. Other 1TCT specimens of low–alloy steel were also in the T–L orientation.

[b]A533–Gr B Class 1 plate (Heat No. A–1195–1) was obtained from the Oak Ridge National Laboratory HSST Program.

[c]Nominal composition of undiluted Inconel–182 weld metal (AWS Type ENiCrFe–3 per AWS Specification A5.11). A layer, ≈6 mm in thickness, was buttered to the A533–Gr B plate using 3/32–in.–diameter weld rod and the material was heat treated at 621°C for 24 h and air–cooled. Inconel–600 (Heat No. NX5922–G11) was electron–beam–welded to the Inconel–182 to form the 1TCT specimen. Entire specimen was nickel–plated.

2.1.2 Results

Results from the SCC tests on the composite specimen are given in Tables 2 and 3, and crack length as a function of time over the entire ≈8700–h test duration is shown in Fig. 1. The crack initiated in the Inconel–182 weld cladding and then penetrated into the underlying low–alloy steel. The crack growth in the Inconel–182 weld metal occurred at a rate of 2.3×10^{-10} m·s^{-1} under high–R loading (0.95) with K_{max} ≈30 MPa·m$^{1/2}$, i.e., virtually the same rate as in sensitized Type 304 SS under similar loading conditions. Figure 1 and Tables 2 and 3 show that crack growth in the A533–Gr B steel can be characterized by long periods (>800 h) of relatively slow growth (Table 2) interrupted by short intervals of rapid (transient) crack extension (Table 3). Of the total crack extension of ≈11.0 mm in the low–alloy steel, only 10% (≈1.0 mm) occurred during the periods of slow local growth and 90% (≈10.0 mm) resulted from the isolated transients. The duration of the transients in these tests can only be bounded by the weekly interval used for the compliance measurements. Overall average crack growth rates of ≈1.6 and 6.8×10^{-10} m·s^{-1} were calculated for the time intervals from ≈2000 to 5700 h (K_{max} ≈30–50, ΔK ≈1.5–2.5 MPa·m$^{1/2}$) and ≈5700 to 8700 h (K_{max} ≈50–100, ΔK ≈2.5–5 MPa·m$^{1/2}$), respectively. Significant crack growth appears to occur even at the lowest stress intensities used in the test (30–35 MPa·m$^{1/2}$).

The transient crack jumps, Δa, are given in Table 3. They typically occurred in the week following a ≈10–12% increase in load (stress intensity). However, transient crack growth of ≈2 mm also occurred at the same applied load shortly after the testing resumed following a two–week shutdown (Test No. 5B in Table 3), and with no change in applied load or other variables toward the end of Test No. 7 in Table 2 (crack extension of 1.80 mm in Test No. 8 of Table 3). The transient crack growth rates obtained by dividing the crack extension Δa by the time interval between successive compliance measurements represent

Table 2. Slow Local Crack Growth of Inconel-182/A533-Gr B Composite Specimen[a] under Low-Frequency, High-R Loading[b] in High-Purity Water with ≈200 ppb Dissolved Oxygen[c] at 289°C

Test No.	Time, h	Cond., μS·cm^{-1}	pH at 25°C	Electrode Potential 304 SS, mV(SHE)	Electrode Potential Pt, mV(SHE)	Inconel-182/A533-Gr B K_{max},[d] MPa·m$^{1/2}$	Inconel-182/A533-Gr B ΔK, MPa·m$^{1/2}$	Inconel-182/A533-Gr B Growth Rate, m·s^{-1}
1A	0	0.11	6.54	125	140	28.0		
	1776					29.6		2.31 x 10^{-10} [e]
1B	1943					30.7		
	2447					30.8	1.54	0.13 x 10^{-10} [f]
2	2620	0.10	6.41	130	140	35.0		
	3496					35.9	1.80	0.16 x 10^{-10}
3	3659	0.10	6.42	120	140	40.0		
	4762					42.3	2.12	0.45 x 10^{-10}
4	4925	0.13	6.38	125	130	45.0		
	5768					45.2	2.26	0.18 x 10^{-10}
5A	5939	0.12	6.41	120	120	50.0		
	6271					55.4	2.77	1.09 x 10^{-10}
5B[g]	6439					62.6		
	7206					63.3	3.17	0.63 x 10^{-10}
6	7209	0.11	6.22	120	120	70.8		
	7709					71.5	3.58	0.39 x 10^{-10}
7	7878	0.11	6.30	130	130	80.0		
	8547					90.9	4.55	1.14 x 10^{-10}
	8718					102.1		

[a] Composite compact tension specimen (1TCT) (No. 02C-1) was fabricated from Inconel-600/Inconel-182/A533-Gr B Steel (Heat No. A-1195-1). Specimen was electroplated with nickel.

[b] Frequency of the positive sawtooth waveform was 8 x 10^{-2} Hz; load ratio R was 0.95.

[c] Effluent dissolved-oxygen concentration was ~200 ppb; feedwater oxygen concentration was higher by a factor of 2 to compensate for oxygen depletion by corrosion of the autoclave system.

[d] Stress intensity, K_{max}, value at the end of each time period was increased by ~ 5 MPa (except in tests 1B and 5B).

[e] Crack growth during the first ~1770 h was in the Inconel-182 weld metal.

[f] Crack growth during the last ~500 h was in the underlying A533-Gr B steel.

[g] System was shut down for a two-week period and the test (5B) was resumed at this time under the previous loading condition.

lower bound values, because the crack extension could have occurred within a shorter time period.

At the end of the test, the specimen was sectioned for metallographic examination. Figure 2 shows a transverse section of the specimen at the half-width, the fracture surface of half the specimen, the crack path at low magnification, and SEM photographs of the

Table 3. Transient Crack Growth of Inconel-182/A533-Gr B Composite Specimen[a] under Low-Frequency, High-R Loading[b] in High-Purity Water with ≈200 ppb Dissolved Oxygen[c] at 289°C

Test No.	Time, h	Cond., μS·cm^{-1}	pH at 25°C	Electrode Potential 304 SS, mV(SHE)	Electrode Potential Pt, mV(SHE)	Inconel-182/A533-Gr B K_{max}, MPa·m$^{1/2}$	Inconel-182/A533-Gr B ΔK, MPa·m$^{1/2}$	Inconel-182/A533-Gr B d_f,[d] mm	Inconel-182/A533-Gr B d_m,[e] mm	Inconel-182/A533-Gr B Crack (a), mm	Inconel-182/A533-Gr B Δa, mm	Inconel-182/A533-Gr B Δt, h	Inconel-182/A533-Gr B Growth Rate,[f] m·s^{-1}
1	1776	0.11	6.54	125	140	29.6	1.48			4.11			
	1943					30.7	1.54	3.3×10^{-4}	0.56	4.90	0.79	167	1.31×10^{-9}
2	2447	0.10	6.41	130	140	30.8	1.54			4.93			
	2620					35.0	1.75	4.6×10^{-4}	0.74	5.36	0.43	173	0.69×10^{-9}
3	3496	0.10	6.42	120	140	35.9	1.80			5.44			
	3659					40.0	2.00	6.0×10^{-4}	0.97	6.38	0.94	163	1.60×10^{-9}
5A	5768	0.12	6.41	120	120	45.2	2.26			6.63			
	5939					50.0	2.50	9.4×10^{-4}	1.50	8.48	1.85	171	3.01×10^{-9}
5B[g]	6271					55.4	2.77			8.61			
	6439					62.6	3.13	1.5×10^{-3}	2.36	10.85	2.24	168	3.70×10^{-9}
7	7709	0.11	6.30	130	130	71.5	3.58			11.18			
	7878					80.0	4.00	2.4×10^{-3}	3.83	13.03	1.85	169	3.04×10^{-9}
8	8547					90.9	4.55			13.31			
	8718					102.1	5.10	3.9×10^{-3}	6.24	15.11	1.80	171	2.92×10^{-9}

[a]Composite compact tension specimen (1TCT) (No. 02C-1) was fabricated from Inconel-600/Inconel-182/A533-Gr B Steel (Heat No. A-1195-1). Specimen was electroplated with nickel.

[b]Frequency of the positive sawtooth waveform was 8×10^{-2} Hz; load ratio R was 0.95.

[c]Effluent dissolved-oxygen concentration was ~200 ppb; feedwater oxygen concentration was higher by a factor of 2 to compensate for oxygen depletion by corrosion of the autoclave system.

[d]Cyclic plastic zone size given by the equation: $d_f = (1/3\pi)(\Delta K/2\sigma_y)^2$, where σ_y is the yield stress of the steel at 289°C, viz., 420 MPa.

[e]Monotonic plastic zone size given by the equation: $d_m = (1/3\pi)(K_{max}/\sigma_y)^2$.

[f]Transient crack growth rate during a time period of ≤170 h between consecutive compliance measurements after increasing the load (by ~3.5 kN or ~12% of the applied load) at the end of each test period (except in tests 1B and 5B) in Table 2. Incremental crack growth could have occurred within a smaller time period; consequently, these are minimum values.

[g]System was shut down for a two-week period and the test (5B) was resumed at this time under the previous loading condition.

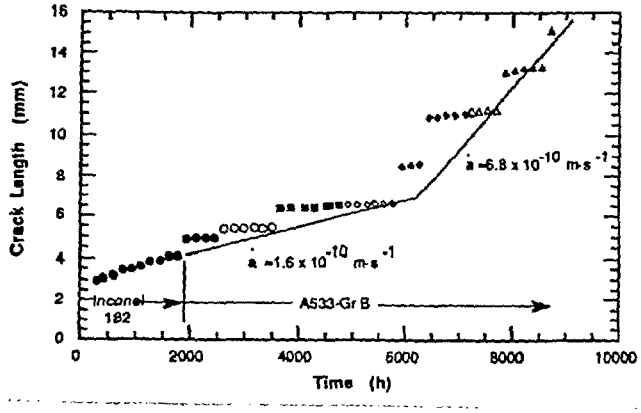

Fig. 1.
Crack Length vs. Time for a 1TCT Composite Inconel-182/A533-Gr B Specimen in High-Purity Oxygenated (≈200 ppb) Water at 289°C.

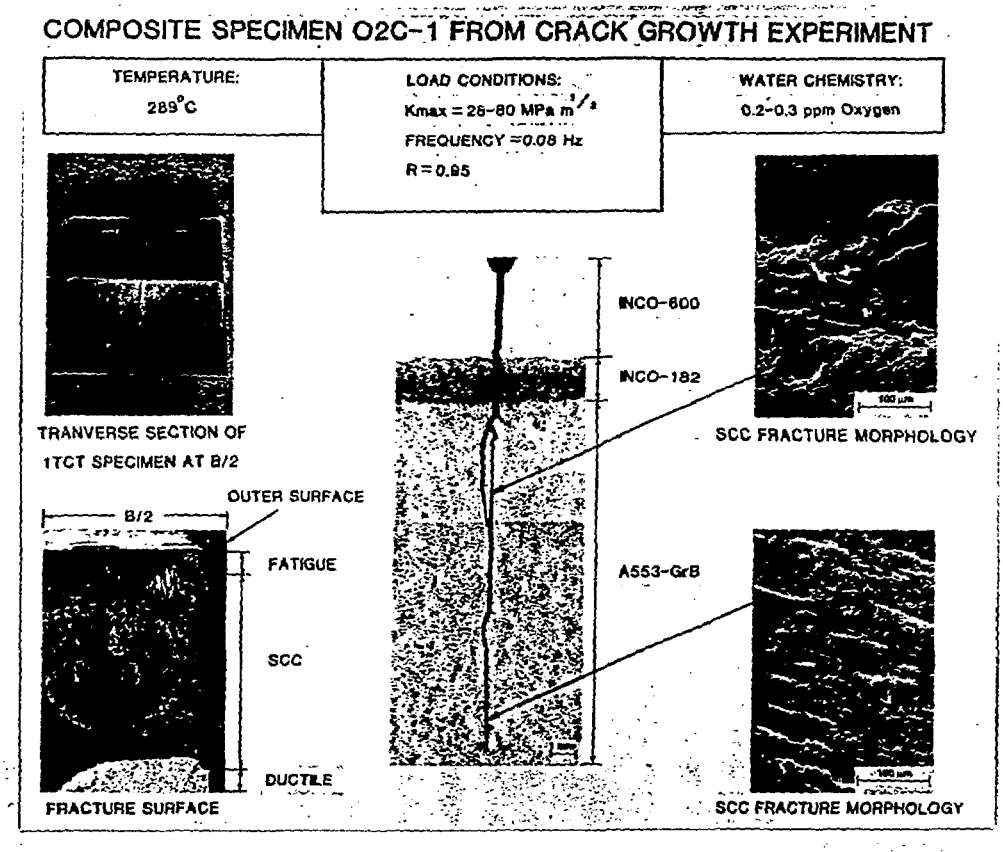

Fig. 2. Fracture Surface and SCC Fracture Morphology of a 1TCT Composite Inconel-182/A533-Gr B Specimen after a Crack Growth Experiment in High-Purity Oxygenated (≈200 ppb) Water at 289°C.

fracture surface at two locations along the crack. Figure 3 is photomicrograph of the crack path at higher magnification, which shows corrosion of the A533–Gr B steel. The heat affected zone (HAZ) of several grain diameters in the low–alloy steel and the fracture surface morphology in the vicinity of the Inconel–182/A533 Gr B weld interface are shown in Fig. 4. The hardness of the HAZ (Rockwell hardness R_B 106) was only slightly greater than the base metal (Rockwell hardness B 96) after the post–weld heat treatment at 621°C for 24 h and air cooling.

In general, the entire fracture surface of the A533–Gr B steel was featureless in comparison with those observed by other investigators[9–13] in tests at lower R values. There is no evidence of the planar facets, striations parallel to the crack front, secondary cracking, and deep ridges perpendicular to the crack front that appear to be characteristic of very high growth rates, at least at low R values.[10] The corrosion product was removed from the fracture surface by immersing the specimen in a cleaning solution (2 g of hexamethylene tetramine in 1 L of 1N HCl) for 30 to 180 s at room temperature. The duration of this test was very long (≈1 y) compared to the duration of tests at low R values, and it is possible that planar facets and striations, if present, could have been obscured by corrosion during the long exposure to the environment. As shown in Fig. 5, "beach marks" were noted on the fracture surface and their location in most instances could be correlated with increases in load and subsequent transient crack growth.

The results of these tests may be compared with those obtained in a similar experiment on an A508 Cl 2 steel with a Type 308 SS weld clad in simulated BWR water with 200 ppb dissolved oxygen at 270°C at lower R and K_{max} levels.[13] Under R = 0.7, low–frequency loading at K_{max} = 25 MPa·m$^{1/2}$ crack growth occurred at ≈3.2 x 10^{-8} m·s^{-1}; at R = 0.1, crack arrest (or propagation at a very low rate) occurred for K_{max} = 16.5 MPa·m$^{1/2}$, and growth occurred at ≈1.1 x 10^{-8} m·s^{-1} for K_{max} = 25 MPa·m$^{1/2}$.

A533–Gr B specimens without plating and those plated with either nickel or gold were tested simultaneously in the same autoclave in simulated BWR water containing ≈200 ppb dissolved oxygen. The CGR results are summarized in Tables 4 and 5. A number of different R values were tested. As in the case of the composite specimen, at R = 0.95 long periods of slow local crack growth were observed (Table 4) interrupted by bursts of transient crack growth (Table 5, Fig. 6). For R = 0.95, no crack growth occurred in either the unplated or plated specimens for maximum stress intensity values of <40 MPa·m$^{1/2}$.

It is difficult to deduce from the present results a consistent picture of the effect of the cladding. The steady–state CGRs in the gold– and nickel–plated specimens in Test No. 1 at an R value of 0.25 (Table 4) were significantly higher than that in the unplated specimen. At an R value of 0.5, the CGRs of the unplated and plated specimens were essentially the same (4 to 7 x 10^{-8} m·s^{-1}). At an R value of 0.8, CGRs in the plated specimens (≈3 x 10^{-8} m·s^{-1}) were again much higher than in the unplated specimen (below resolution). Because crack lengths in the plated specimens were now significantly greater than that in the unplated specimen, there was a substantial disparity in K values for the remainder of the test and further comparisons were not meaningful. On the basis of these limited results, it appears that

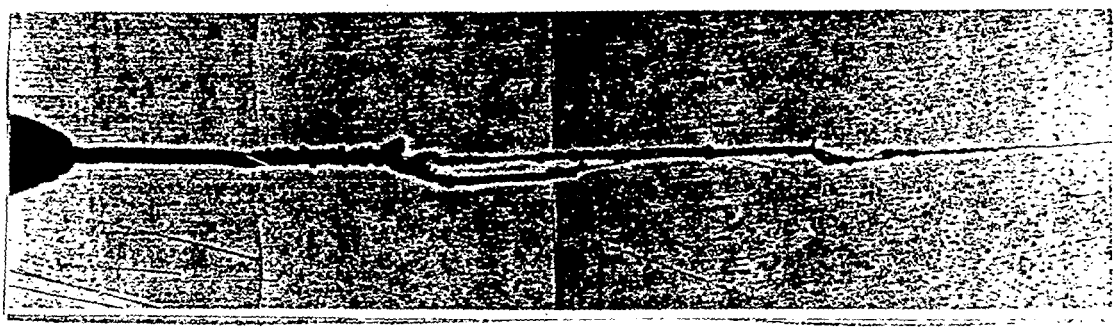

Fig. 3. Crack Path at a Higher Magnification, Showing Corrosion of Crack Surfaces.

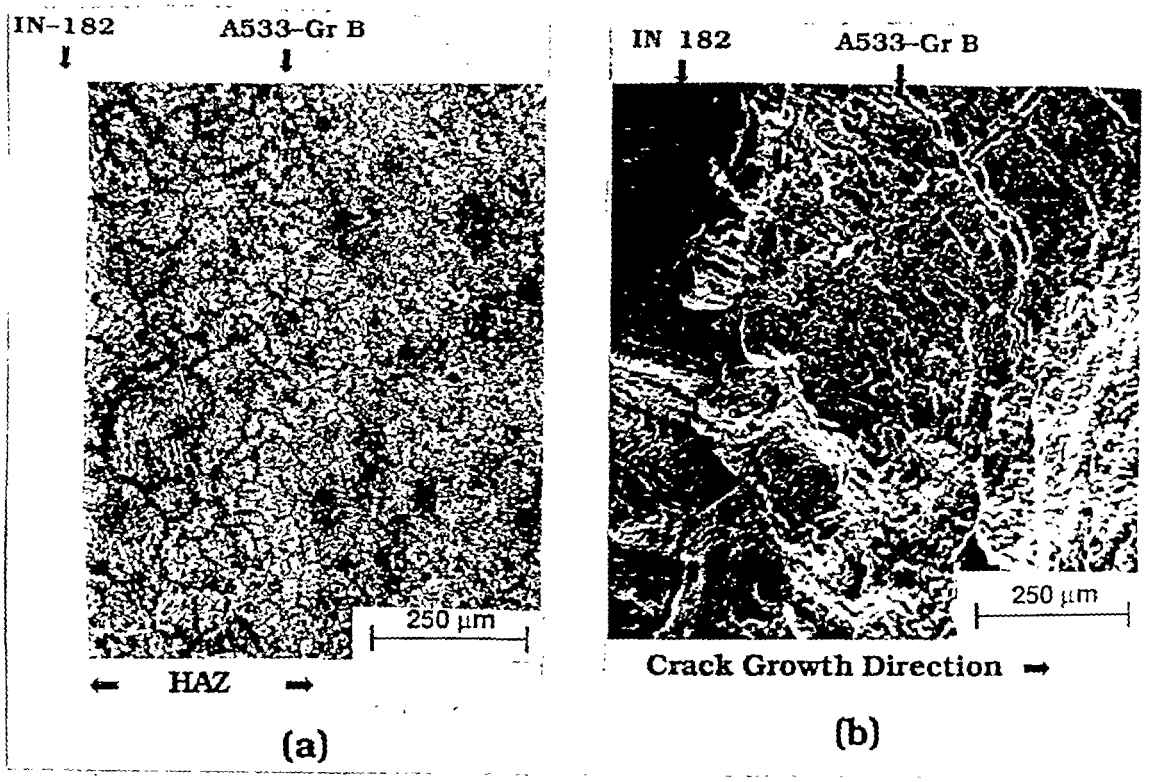

Fig. 4. (a) Heat-Affected Zone (HAZ) in A533-Gr B Steel and (b) Fracture Surface in Vicinity of Inconel/182/A533-Gr B Interface after CGR Test in Simulated BWR Water at 289°C.

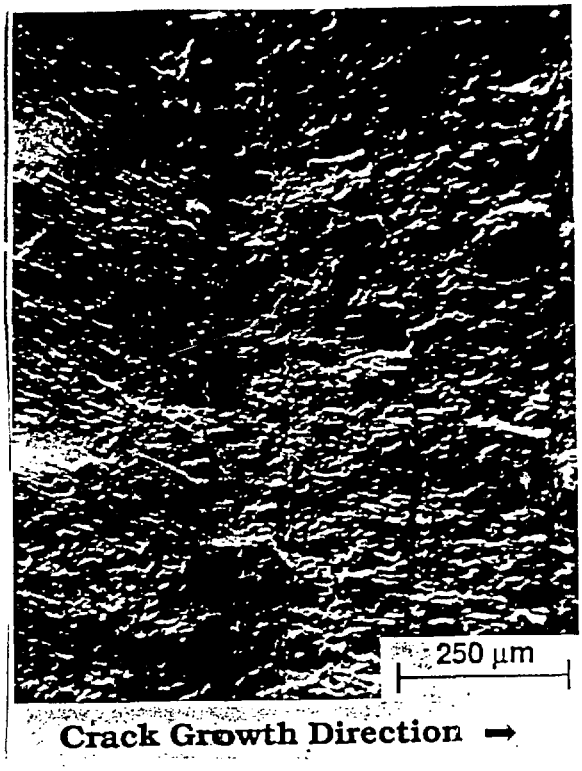

Fig. 5.
"Beach" Marks on Fracture Surface of A533-Gr B Steel.

the nature of the surface layers on the specimen, either different oxides (Fe_3O_4 vs. NiO) or a noble metal (gold) influences the crack growth behavior of the low-alloy steel in oxygenated water; further investigation, however, is planned.

The CGRs in the plated specimens decreased significantly when R was increased to 0.9 and decreased further when R was increased to 0.95. However, as in the case of the composite specimen, these low CGRs are misleading, because under the high-R loading most of the crack growth occurs during brief transients. Transient crack growth occurred in the unplated A533-Gr B specimen at an R value of 0.95 (Table 5), but only at K values of 40-50 $MPa \cdot m^{1/2}$. The transient crack extensions, Δa, and the time intervals over which they occurred are given in Table 5, along with the transient crack growth rates. The rates are comparable to those for the composite specimen in Table 3. The amount of crack extension that occurred during time intervals of ≈30 h (i.e., ≈0.2 mm) is much less than that observed in the composite specimen or the monotonic plastic zone size calculated by Eq. 1. However, it may be only that the continuous monitoring reveals that the transients actually proceed by a series of smaller jumps, and if the total extension is considered over a time period comparable to the ≈170-h intervals between compliance measurements, the results are more comparable. The composite specimen also received an additional periodic cyclic loading during the compliance measurements, and this may affect susceptibility to transient crack growth.

Table 4. Steady-State Crack Growth of A533-Gr B Specimens[a] at Several R Values[b] in 289°C Water[c] with ≈200 ppb Dissolved Oxygen and 100 ppb Sulfate

Test No.	Time, h	Cond., $\mu S \cdot cm^{-1}$	Electrode Potentials		Load Ratio	Nonplated (No. 02C-04)		Nickel-plated (No. 02C-05)		Gold-plated (No. 02C-06)	
			A533-Gr B, mV(SHE)	Pt, mV(SHE)		K_{max}[d], $MPa \cdot m^{1/2}$	Growth Rate, $m \cdot s^{-1}$	K_{max}[d], $MPa \cdot m^{1/2}$	Growth Rate, $m \cdot s^{-1}$	K_{max}[d], $MPa \cdot m^{1/2}$	Growth Rate, $m \cdot s^{-1}$
1	0 46	0.12	-94	33	0.25	20.9	3.8×10^{-9}	20.8	3.8×10^{-9}	22.7	1.8×10^{-8}
2	46 913	0.12	-58	35	0.95	20.9	–[e]	20.8	–	22.7	–
3	913 1200	0.13	-40	69	0.95	22.9	–	22.9	–	25.5	–
4	1201 1491	0.14	-36	93	0.95	25.0	–	25.0	–	27.8	–
5	1494 1798	0.14	-58	71	0.95	30.5	–	30.5	–	33.8	–
6	1800 1821	0.13	-63	43	0.50	36.5	6.2×10^{-8}	37.7	7.0×10^{-8}	39.5	4.3×10^{-8}
7	1824 2161	0.23	-61	77	0.95	37.8	–	39.2	–	40.2	–
8	2162 2232	0.23	1	83	0.80	37.8	–	58.2	3.0×10^{-8}	50.1	2.3×10^{-8}
9	2233 2306	0.17	-34	81	0.90	37.8	–	59.0	3.8×10^{-10}	51.0	6.0×10^{-10}
10	2307 2711	0.16	-80	-4	0.95	37.8	–	59.0	–	51.3	2.4×10^{-11}
11	2712 2976	0.14	1	92	0.95	37.8	–	59.0	–	51.4	3.1×10^{-11}
12	2979 3148	0.12	47	97	0.95	44.1	–	68.7	–	60.1	8.8×10^{-11}
13	3152 3486	0.14	34	68	0.95	49.7	3.9×10^{-10}	75.7	–	66.9	–
14	3488 3888	0.17	26	82	0.95	49.7	–	75.7	–	69.9	6.7×10^{-9}

[a]Heat No. A-1195-1. Crack plane orientation was the T-L direction.

[b]Frequency of the positive sawtooth waveform was 8×10^{-2} Hz.

[c]Effluent dissolved-oxygen concentration was ≈200 ppb; feedwater oxygen concentration was approximately an order of magnitude higher to compensate for oxygen depletion by corrosion of the autoclave system.

[d]Stress intensity, K_{max}, values at the end of the time period.

[e]No significant crack growth or no measurement.

Table 5. Transient Crack Growth of A533-Gr B Compact Tension Specimens[a] under Low-Frequency, High-R Loading[b] in Water[c] with ≈200 ppb Dissolved Oxygen at 289°C

Test No.	Time, h	Cond., $\mu S \cdot cm^{-1}$	Electrode Potentials: 304 SS, mV(SHE)	Electrode Potentials: Pt, mV(SHE)	A533-Gr B: K_{max}, $MPa \cdot m^{1/2}$	A533-Gr B: ΔK, $MPa \cdot m^{1/2}$	A533-Gr B: d_f,[d] mm	A533-Gr B: d_m,[e] mm	A533-Gr B: Crack (a), mm	A533-Gr B: Δa, mm	A533-Gr B: Δt, h	A533-Gr B: Growth Rate,[f] $m \cdot s^{-1}$
Specimen No. 02C-04 (Nonplated)												
1	2975	0.12	38	122	37.7	1.89			22.77			
	2979				44.0	2.20	7.3×10^{-4}	1.18	22.82	0.05	4	3.5×10^{-9}
2	3152	0.12	47	68	48.5	2.43			22.84			
	3161				48.6	2.43	8.9×10^{-4}	1.41	22.88	0.04	9	1.2×10^{-9}
3	3196	0.11	21	63	48.6	2.43			22.86			
	3232				49.2	2.46	9.1×10^{-4}	1.44	23.11	0.25	36	1.9×10^{-9}
4	3356	0.11	25	75	49.3	2.47			23.13			
	3386				49.8	2.49	9.3×10^{-4}	1.50	23.30	0.17	30	1.6×10^{-9}
Specimen No. 02C-06 (Gold-plated)												
1	3148	0.12	55	75	60.1	3.01			27.94			
	3153				66.8	3.34	1.7×10^{-3}	2.68	28.09	0.15	5	8.3×10^{-9}

[a]Heat No. A-1195-1. Crack plane orientation was the T-L direction.

[b]Load ratio and frequency of the positive sawtooth waveform were 0.95 and 8×10^{-2} Hz, respectively.

[c]Effluent dissolved-oxygen concentration was ≈200 ppb; feedwater oxygen concentration was approximately an order of magnitude higher to compensate for oxygen depletion by corrosion of the autoclave system.

[d]Cyclic plastic zone size given by the equation: $d_f = (1/3\pi)(\Delta K/2\sigma_y)^2$, where σ_y is the yield stress of the steel at 289°C, viz., 420 MPa.

[e]Monotonic plastic zone size given by the equation: $d_m = (1/3\pi)(K_{max}/\sigma_y)^2$.

[f]Average crack growth rate for the time interval determined by the DC potential drop technique.

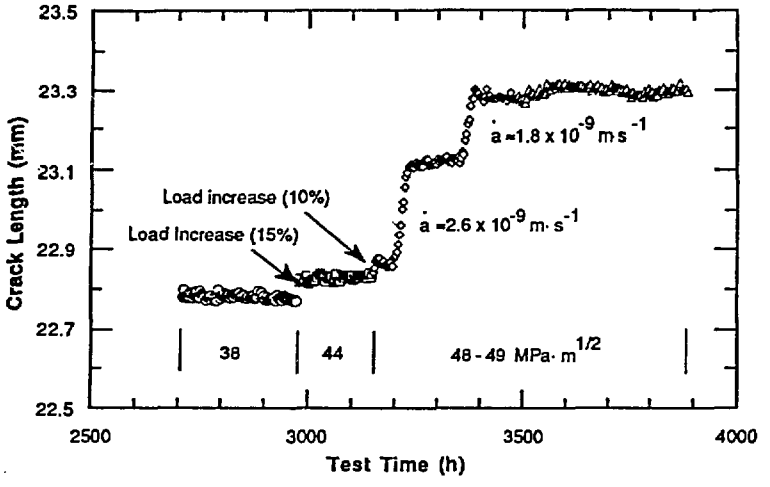

Fig. 6. Slow and Transient Crack Growth in Unplated A533-Gr B Specimen under R = 0.95 Loading.

After testing, the unplated and plated specimens were fractured to examine the nature of the fracture surface and to compare the final crack lengths with those determined by the DC potential drop technique. As in the case of the composite specimen, the fracture surfaces were relatively featureless. However, in the gold-plated specimen where rapid crack growth occurred near the end of the test, fan-shaped, brittle-fracture regions similar in character to those associated with MnS inclusion sites in previous tests on slow-strain-rate specimens[14] were observed. The average crack lengths from measurements on the fracture surface were within 3% of the values obtained by the DC potential drop measurements during the tests.

The most striking feature of the current tests is the periodic bursts of rapid transient crack growth. Other investigators have also observed crack growth spurts of several millimeters in low-alloy steels within ≈50 to 100 h after incremental increases in load or decreases in frequency, test interruptions, changes in environmental conditions, and for unknown reasons (particularly in tests at high R values).[9,10,15] Such transients are generally observed only in materials containing MnS particles. Although the actual process(es) responsible for transient growth remain(s) unidentified, several mechanisms have been suggested.[16] Dissolution of MnS particles at the crack tip provides an aggressive environment that could lead to enhanced crack growth because either (1) the dissolved sulfides decrease the repassivation rate which increases the amount of metal dissolution for a given oxide rupture rate, or (2) the dissolved sulfides poison the recombination of hydrogen atoms liberated by corrosion, which enhances hydrogen uptake by the steel at the crack tip. Although in some cases it has been conjectured that the crack jumps can be associated with thumbnail-shaped, brittle-fracture regions on the fracture surface, it is difficult to distinguish between these and other possible mechanisms on the basis of fractographic evidence or studies of MnS concentration and distribution in the steel.

In a previous study, it was observed that the size of the transient crack jump was comparable to that of the monotonic plastic zone ahead of the crack (and was generally much larger than the cyclic plastic zone).[10] Because hydrogen accumulation ahead of the crack tip would tend to localize in the zone of high plastic deformation, this suggests that a hydrogen-assisted cracking mechanism could be responsible for the transient growth. To test these hypotheses in the present tests, the monotonic and cyclic plastic zone sizes, d_m and d_f, respectively, were calculated for the crack length and stress intensity at which transient crack growth occurred, using the estimate for d_m developed by Irwin:[17]

$$d_m = 2r_y = \frac{1}{3\pi}\left(\frac{K_{max}}{\sigma_y}\right)^2 \tag{1}$$

$$d_f = 2r_f = \frac{1}{3\pi}\left(\frac{\Delta K}{2\sigma_y}\right)^2 \tag{2}$$

The results in Table 3 show that the calculated monotonic plastic zone sizes are similar in magnitude to the observed crack extensions except when the stress intensity factors are very high and the validity of the small-scale yielding formula (Eq. 1) is questionable.

Fatigue crack growth rate reference curves for A533-Gr B and related weld materials in LWR environments, which can be used to calculate crack growth under cyclic loading, are provided in the ASME Boiler and Pressure Vessel Code, Section XI, Appendix A. The evolution of these from 1972 to the present has been reviewed by Bulloch.[16] Fatigue crack growth data for these materials in air can be reasonably well represented by a power-law relationship between crack growth per cycle, $\frac{da}{dN}$, and stress intensity range, ΔK. Initially it was proposed that the CGRs in the environment simply be taken as roughly an order-of-magnitude higher than the rates in air. Studies in the 1970s showed that there was a large effect of load ratio that was not reflected in this approach, and the Code was revised in 1980 to incorporate experimental data generated in the interim; this decreased the ΔK threshold value at which cracking can occur at higher R values.

Subsequent studies have shown that the 1980 curves do not always accurately describe fatigue crack growth behavior.[18] Recent work has shown that environmentally assisted cracking is more consistently described in terms of time-based crack growth, $\frac{da}{dt}$, as a function of crack-tip strain rate where the crack tip strain under cyclic loading can be considered proportional to $\frac{da}{dt}$ in an inert environment (air).[19-22] Although time-based CGRs are more fundamental, the resulting correlations have been recast in terms of the more familiar $\frac{da}{dN}$ (although the curves are now frequency- [rise-time] dependent) and are currently being considered for inclusion in Section XI of the Code.[23]

The average, local, and transient CGRs from the tests on the composite A533-Gr B/Inconel-182 specimen (Tables 2 and 3 and Fig. 1) and the CGRs from the unplated and plated specimens under R = 0.95 loading (Table 4) are compared in Fig. 7 with the high-R (R >0.65) curve for water and the "air line" from the 1980 version of ASME Section XI, as well as with a revised air line.[24] The local CGRs fall close to the revised air line, and appear to be representative of cyclic crack growth under R = 0.95 loading when environmental effects are relatively unimportant. The transient and overall average CGRs for R = 0.95, not unexpectedly, lie considerably above the ASME Section XI (1980) high-R water line.

The proposed revised ASME Section XI $\frac{da}{dN}$ vs ΔK curves* were used to calculate equivalent $\frac{da}{dt}$ vs. K_{max} curves. The CGR results on the composite and gold-plated specimens at R = 0.95 and the data from Prater,[4] Hale,[6] and Van der Sluys** at R = 1 are compared in Fig. 8 with the Section XI curve for R = 0.95 and a rise time of 12 s. As noted previously the "local" crack growth rates lie close to the Code predictions for crack growth when environmental effects are relatively unimportant. Both the transient and overall average crack growth rates in the present tests and the data of Prater, Hale, and Van der Sluys at R = 1 are well above the predicted curves. If the threshold for the onset of environmentally accelerated cracking is shifted as indicated by the dashed curve in Fig. 8, the magnitude of the environmentally accelerated cracking is in reasonable agreement with the Code prediction for all the data with 200 ppb dissolved oxygen in water.

The shift in the threshold is consistent with the notion that environmentally accelerated cracking depends strongly on the crack tip strain rate. The Code equations in essence assume that the crack tip strain rate is dominated by the cyclic loading and ignore any contributions from time-dependent deformation processes under R = 1 loading. Current empirical estimates of the crack tip strain rate[25] suggest that for R ≤0.9, cyclic loading dominates the crack tip strain rate, but at R ≥0.95, time-dependent processes dominate. This is also consistent with the data shown in Fig. 8, which suggest that the threshold stress intensity needed to obtain environmentally accelerated cracking appears to be similar for tests at R = 0.95 and 1. The data obtained at lower R values are compared with the Code predictions in Fig. 9. Even for the plated specimens at R = 0.9, the data are in reasonably good agreement with the predictions.

Fatigue of Type 316NG SS

Residual-life assessment reviews for LWRs indicate that low-cycle fatigue is a potentially significant degradation mechanism in LWR primary piping. This degradation mechanism must be considered when justifying extended operation of an LWR plant.[26] Current fatigue design for austenitic SS piping is based on the ASME Section III Fatigue Design Curves. Environmental effects are not explicitly considered in these curves. Instead, the design

---

*The proposed curves have undergone a number of revisions. The versions used here are those presented to the Subgroup on Fatigue Strength at the February 5, 1990, meeting in New York City.

**A. Van der Sluys, Presentation at ICCGR Meeting, Jekyll Island, South Carolina, August 10-11, 1989.

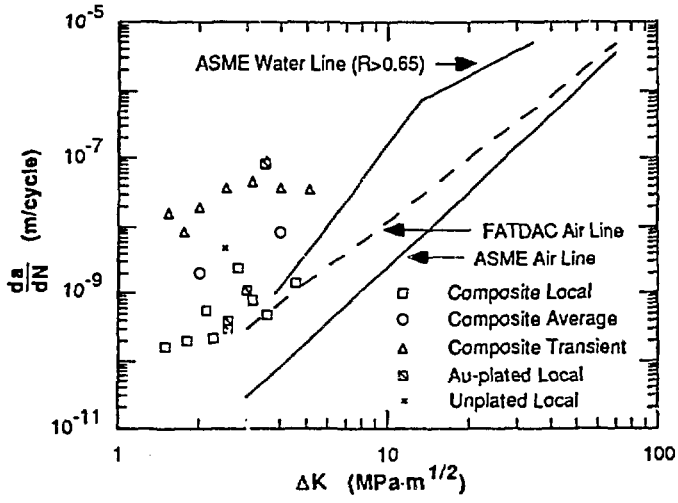

Fig. 7.
Average, Local, and Transient CGRs from Tests on Composite A533-Gr B/Inconel-182 and Gold-Plated Specimens, ASME Section XI (1980) Curves for Water (R >0.65) and Air, and a Revised[24] "Air Line."

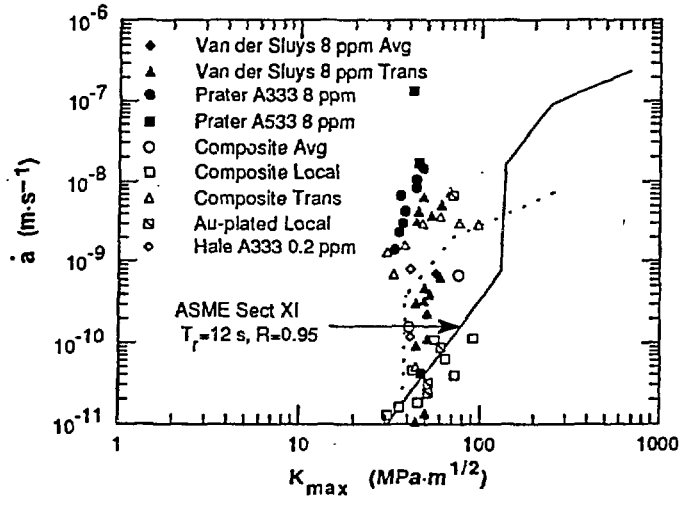

Fig. 8.
CGR Results from Composite A533-Gr B/Inconel-182 and Gold-Plated Specimens, from other Investigations on Low-Alloy Steels at R = 1 Loading,[4,6] and Proposed[23] ASME Section XI Curve for R = 0.95 in a Time-Based $\frac{da}{dt}$ vs K_{max} Format.

curves are obtained by introducing a factor of 2 on the strain range or 20 on the cycles from the mean life curve, whichever is more conservative. Several studies have shown that the effect of typical BWR water on the fatigue life of A106-Gr B and A333-Gr 6 steel can completely erode the "2 or 20" margin in the Code Design Curve.[27-29] In-reactor tests showed that the fatigue life of sensitized SS was significantly shorter in BWR environments, but relatively little effect was observed on nonsensitized stainless steels, at least at the high strain ranges tested.

The objective of the current work is to provide additional information on the effects of operating temperature and environment on the fatigue behavior of Type 316NG SS. The data are needed to assess the degree of conservatism inherent in the ASME Code Section III

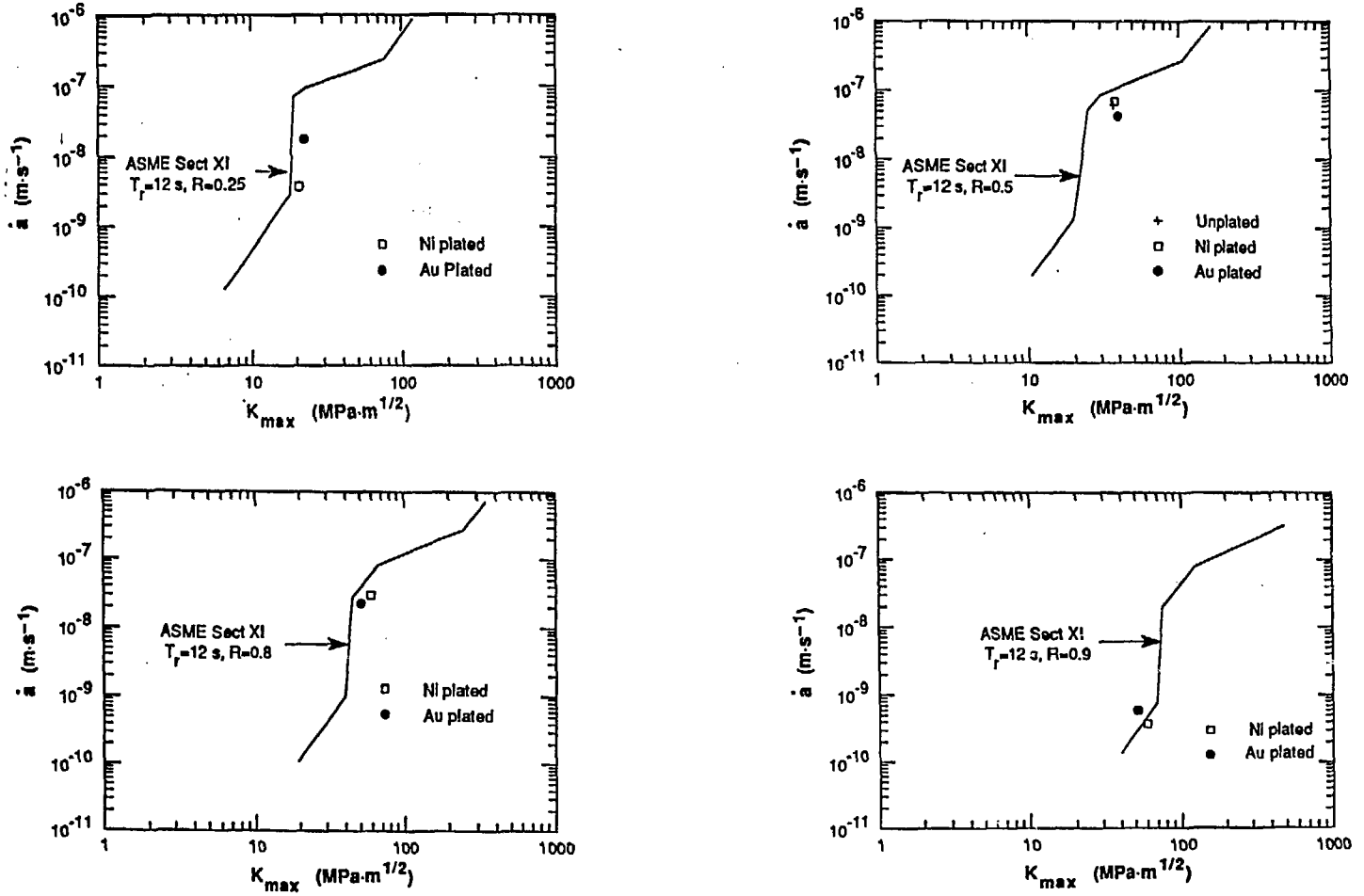

Fig. 9. CGR Results from Conventional (unplated) and Nickel- and Gold-Plated A533-Gr B Specimens at Several R Values (0.25 to 0.9) and Proposed[23] ASME Section XI Curves in a Time-Base $\frac{da}{dt}$ versus K_{max} Format.

Fatigue Design Curves for this material. They may also be needed for decisions on life extension beyond the current 40-year design life.

Test procedures and specimen design are described in Ref. 30. Baseline tests were performed in air at room temperature (22°C) and at reactor operating temperatures (288 and 320°C). The tests were performed in high-purity water with ≈200 ppb dissolved oxygen at 288°C. The results of the tests in air and in the simulated BWR environment are summarized in Table 6.

As shown in Fig. 10, at cyclic strain ranges ≥0.5% there is relatively little effect of temperature on fatigue life in air over the temperature range of interest in LWRs. However, at lower cyclic strain ranges, fatigue life at 288 and 320°C is significantly lower than that at room temperature. At 0.25%, the lowest strain range tested, the life at 288°C is $\approx\frac{1}{6}$ that at room temperature.

As shown in Fig. 11, at cyclic strain ranges ≥0.30%, fatigue life in simulated BWR water is lower than that in air at the same temperature. Life in the environment decreases with frequency. At 0.005 Hz, the lowest frequency tested, life in water was $\approx\frac{1}{4}$ that in air. For cyclic strain ranges ≥0.30%, the normalized fatigue life N_{env}/N_{air} is relatively independent of strain range and depends primarily on the strain rate. In Fig. 12, these results are compared with similar data obtained by Iida et al.[29] for an A333-Gr 6 steel in water with 8 ppm dissolved oxygen. The A333-Gr 6 steel shows a stronger strain rate dependence and a more severe reduction in fatigue life. However, at a cyclic strain of 0.25%, life in simulated BWR water is ≈7 times that observed in air at 288°C.

In the cyclic strain range regime where the environment is detrimental, fatigue life is dominated by crack growth. The decrease in fatigue life for these cyclic strain ranges is consistent with the increase in crack growth rates in precracked Type 316NG SS specimens that is observed in BWR environments.[31] At the low cyclic strain ranges where life in the environment appears to increase, fatigue life is dominated by the time required to initiate a crack. We can conjecture that corrosion somehow disrupts the formation of an initiation site. In air, an increase in temperature seems to have a contrary effect, i.e., the fatigue life is unaffected for cyclic strain ranges where fatigue life is dominated by crack growth, but life decreases significantly at lower cyclic strain ranges when it is dominated by initiation.

In Fig. 13, the fatigue lives obtained in the present tests are compared with the ASME Section III mean data and design curves for austenitic stainless steels. The ASME mean data curves are based on tests in air. There is good agreement between the in-air tests and the mean data curve for cyclic lives less than 10^5 cycles, but the current data fall below the ASME mean data curve at longer lives. Similar behavior was also observed in Japanese studies on Type 304 and 316LN SS.[32] The ASME design curve reduces the life by a factor of 2 on strain range or 20 on cyclic life, whichever is more conservative. This margin is intended to account at least partially for some environmental effects, surface finish effects, etc. Even in air at room temperature, the design margins are smaller than intended for strain ranges between 0.25 and 0.5%. In BWR environments at sufficiently low frequencies, the margins are further reduced.

Table 6. Comparison of Fatigue Lives of Type 316NG SS in Air and Simulated BWR Water

Test No.	Environment	Temp., °C	Strain Range, %	Frequency, Hz	Cycles to Failure
1390	Air[a]	22	0.75	0.33	25,736
1391	Air[a]	22	1.0	0.33	13,561
1392	Air[a]	22	0.5	0.33	60,741
1393	Air[a]	22	0.4	0.33	127,386
1394	Air[a]	22	1.5	0.33	4,649
1395	Air[a]	22	0.35	0.33	183,979
1396	Air[a]	22	0.75	0.33	30,000
1397	Air[a]	22	0.30	0.33	347,991
1398	Air[a]	22	0.27	0.33	≈666,000
1399	Air[a]	22	0.25	0.33	>1,900,000[b]
1400	Air[a]	22	0.25	0.33	≈1,775,000
1420	Air[c]	22	0.5	0.5	54,249
1407	Air[a]	288	0.4	0.33	82,691
1408	Air[a]	288	0.75	0.33	21,548
1409	Air[a]	288	0.5	0.5	53,194
1410	Air[d]	288	0.5	0.5	51,194
1430	Air[a]	288	0.30	0.33	168,852
1435	Air[a]	288	0.25	0.33	314,352
1480	Air[d,e]	288	0.25	0.33	319,308
1485	Air[d]	288	0.25	0.33	369,206
1404	Air[a]	320	0.5	0.33	47,011
1405	Air[a]	320	0.75	0.33	20,425
1406	Air[a]	320	0.4	0.33	82,691
1414	Water[f]	288	0.5	0.5	26,230
1418	Water[f]	288	0.5	0.5	25,714
1423	Water[f]	288	0.5	0.05	17,812
1425	Water[f]	288	0.5	0.005	13,684
1426	Water[f]	288	0.75	0.5	12,069
1427	Water[f]	288	0.75	0.05	6,679
1428	Water[f]	288	0.75	0.005	5,897
1431	Water[f]	288	0.30	0.5	116,754
1434	Water[f]	288	0.30	0.05	40,643
1436	Water[f]	288	0.25	0.5	>1,719,851[g]
1512	Water[f]	288	0.25	0.5	2,633,954[h]

[a] Baseline test under strain control.
[b] The test failed at ≈1,900,000 due to an equipment malfunction.
[c] Baseline test under stroke control.
[d] Baseline test in air under stroke control in the autoclave.
[e] This test had an inadvertent shutdown because of a power bump after 241,320 cycles. During the shutdown, the specimen was strained to ≈0.425%. It was restarted and continued to failure.
[f] High-purity water with 0.2 ppm dissolved oxygen at 288°C.
[g] Manually shut down at 1,719,851 cycles before specimen failure. Frequency switched from 0.05 Hz to 0.5 Hz after 702,022 cycles.
[h] A power bump produced a compression plastic overstrain of ≈0.6% at 2,444,900 cycles.

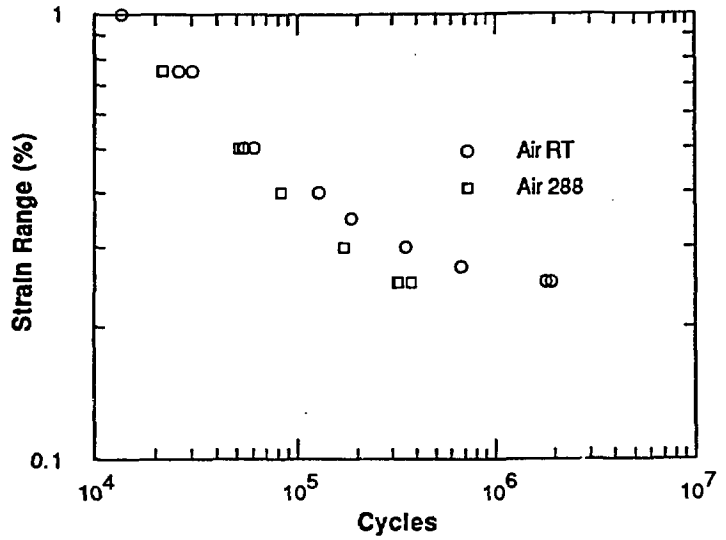

Fig. 10.
Fatigue Life of Type 316NG SS in Air at Room Temperature (22°C) and 288°C.

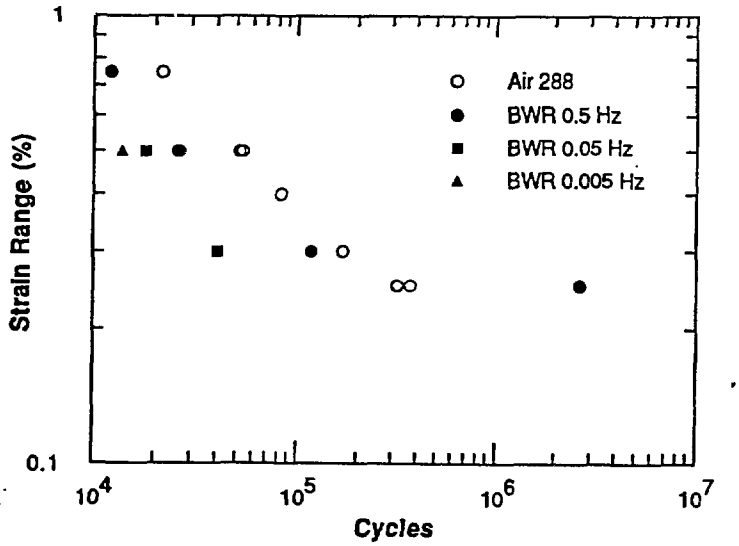

Fig. 11.
Fatigue Life of Type 316NG SS as a Function of Frequency in Water with 200 ppb Dissolved Oxygen and Air at 288°C.

The current series of tests has examined the crack growth behavior of a heat (No. 46113) of modified Type 347 SS and a heat of CF-3 duplex cast stainless steel. The tests were performed in water with 200 ppb dissolved oxygen and 100 ppb sulfate. The compositions of the two heats are given in Table 7, along with the compositions of a heat of modified Type 347 SS and a heat of CF-3M duplex cast stainless steel that were tested previously.

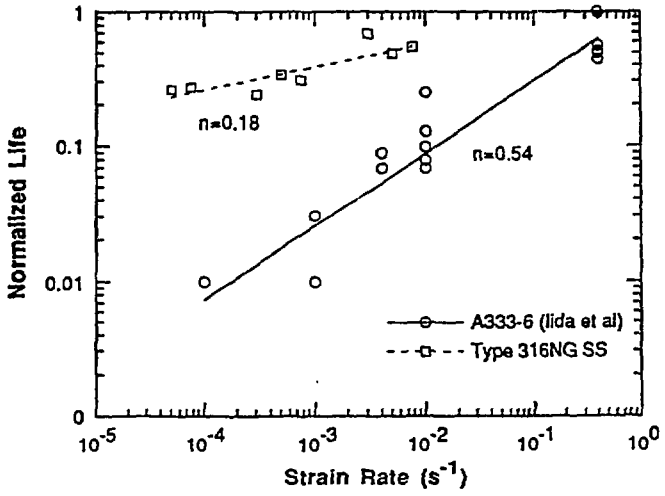

Fig. 12.
Effect of Strain Rate on Normalized Fatigue Life of A333-Gr 6 Steel and Type 316NG SS in Simulated BWR Environments.

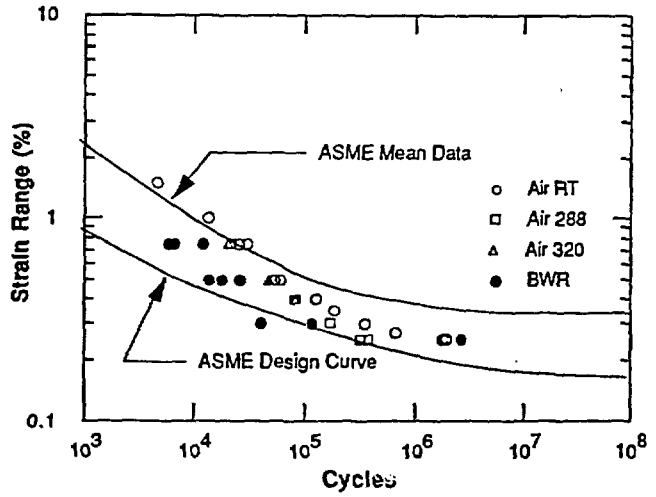

Fig. 13.
Comparison of Fatigue Life of Type 316NG SS in Air and Simulated BWR Water with ASME Section III Mean Data and Design Curves.

The earlier tests of modified Type 347 SS in simulated BWR environments showed that it was very resistant to stress corrosion cracking.[33] The current heat (No. 46113) of modified Type 347 SS was tested in two different heat-treatment conditions, i.e., slow-cooled and water-quenched. The results of the CGR tests are summarized in Table 8. The CGRs in Type 347 SS appear to depend on heat treatment. The rates in material that was solution-heat-treated and water-quenched are typically $\approx\frac{1}{5}$ of those in material that was solution-heat-treated and slow-cooled in air. Both materials show small amounts of grain boundary precipitation. However, neither material indicated sensitization by ASTM A262 Practice A. The water-quenched material was slightly harder (Rockwell hardness R_B 86) than the slow-cooled material (Rockwell hardness R_B 82). Heat treatment has also been shown to affect the SCC susceptibility of modified Type 347 SS in slow-strain-rate tests.[34] In those

Table 7. Chemical Composition and Ferrite Content of Cast Stainless Steels and Composition of Modified Type 347 SS Used in Crack Growth Tests

Grade	Heat	Composition (wt.%)											Ferrite[a] (%)	
		Mn	Si	P	S	Mo	Cr	Ni	N	C	Nb	Cu	Co	Calc.	Meas.
Cast Stainless Steel															
CF-3M	F5524	0.96	1.35	0.015	0.005	2.38	19.38	11.80	0.099	0.018	-	-	-	5.9	5.0
CF-3	P2	0.74	0.94	0.019	0.006	0.16	20.20	9.38	0.040	0.019	-	-	-	12.5	15.6
Modified Type 347 SS															
347	46113	1.21	0.31	0.024	0.013	0.16	17.12	9.65	0.066	0.015	0.23	0.23	0.07	-	-
347	316642	1.56	0.29	0.023	0.014	0.29	18.06	10.81	0.21	0.03	0.60	0.09	-	-	-

[a]Calculated from the composition with Hull's equivalent factor. Measured by ferrite scope AUTO Test FE, Probe Type FSP-1.

tests, the lowest susceptibility was observed in materials that had been solution-heat-treated and slow-cooled, in apparent contrast to the current results. SEM studies suggested that high resistance was associated with a distribution of fine NbC precipitates. In the present studies, in which the heat treatments were performed on large blocks of materials rather than on small specimens, a fine precipitate structure — and consequently higher hardness — is achieved by the water quench, and the precipitate structure coarsens during the slow cool.

The cast stainless steel in the present tests contains ≈15% ferrite. The results in Table 8 show that this material is very resistant to cracking even in the aggressive environment used for the tests. Measurable CGRs under R = 0.95 loading could be obtained only for stress intensity factors >27 MPa·m$^{1/2}$. Previous tests conducted on a specimen of CF-3M steel with a low ferrite content (≈5%) showed a much greater susceptibility to cracking.[35] The differences in susceptibility observed between the two materials are consistent with the variation of susceptibility with carbon and ferrite levels proposed in Ref. 36 and support the suggestion in Ref. 37 that only cast stainless steels with C <0.035 wt.% and ferrite level >8% be considered as highly resistant to cracking.

In Fig. 14, the CGRs in the modified Type 347 SS and the CF-3 duplex are compared with the corresponding CGRs determined from the ASME Section XI reference fatigue crack growth in-air curve for the appropriate temperature and loading conditions. Except for the data at R = 0.5, the Code predictions for the CF-3 steel are generally conservative. The predictions for the Type 347 SS are significantly nonconservative, especially for the slow-cooled material. In Fig. 15, the data are compared with the NRC disposition curve for crack growth in BWR environments under R = 1 loading.[37] The disposition curve gives conservative predictions for all the data at R = 0.9 and 0.95 except for one data point at R = 0.9. The CGRs in the slow-cooled material are comparable to those observed in Type 316NG SS under similar environmental and loading conditions.[31]

Table 8. Steady-State Crack Growth of Type 347 and CF-3 Cast SS 1T Compact Tension Specimens[a] at Several R Values[b] in 289°C Water[c] with ~200 ppb Dissolved Oxygen and 100 ppb Sulfate

Test No.	Time, h	Cond., $\mu S \cdot cm^{-1}$	Electrode Potential		Load Ratio	Slow-Cooled Type 347 SS		Type 347 SS, Slow Cooled		Type 347 SS, Water-Quenched	
			304 SS, mV(SHE)	Pt, mV(SHE)		K_{max}[d], $MPa \cdot m^{1/2}$	Growth Rate, $m \cdot s^{-1}$	K_{max}[d], $MPa \cdot m^{1/2}$	Growth Rate, $m \cdot s^{-1}$	K_{max}[d], $MPa \cdot m^{1/2}$	Growth Rate, $m \cdot s^{-1}$
1	479 524	0.93	150	208	0.5	19.6	2.7×10^{-9}	19.8	–[e]	19.8	3.0×10^{-9}
2	526 788	0.92	147	200	0.9	19.7	8.8×10^{-12}	19.9	8.5×10^{-11}	19.8	9.1×10^{-12}
3	791 986	0.92	121	159	0.9	21.8	4.0×10^{-11}	22.3	3.4×10^{-10}	22.0	1.3×10^{-10}
4	988 1895	0.95	174	223	0.95	21.8	–	22.4	9.3×10^{-12}	22.1	7.5×10^{-12}
5	1896 2207	0.96	185	211	0.95	26.6	–	27.6	1.7×10^{-10}	27.0	6.0×10^{-11}
6	2210 2469	0.92	176	210	0.95	29.2	1.1×10^{-11}	30.7	3.0×10^{-10}	29.8	6.0×10^{-11}
7	2483	0.89	138	174	1.0	29.2	–	31.1	8.9×10^{-11}	30.0	6.1×10^{-11}

[a]Heat Nos. 46113 for Type 347 SS and P2 for CF-3 Cast SS. Crack plane orientation was the L-T direction.

[b]Frequency of the positive sawtooth waveform was 8×10^{-2} Hz.

[c]Effluent dissolved-oxygen concentration was ~200 ppb; feedwater oxygen concentration was approximately five times higher to compensate for oxygen depletion by corrosion of the autoclave system.

[d]Stress intensity, K_{max}, values at the end of the time period.

[e]CGR could not be measured because of instrumentation problem.

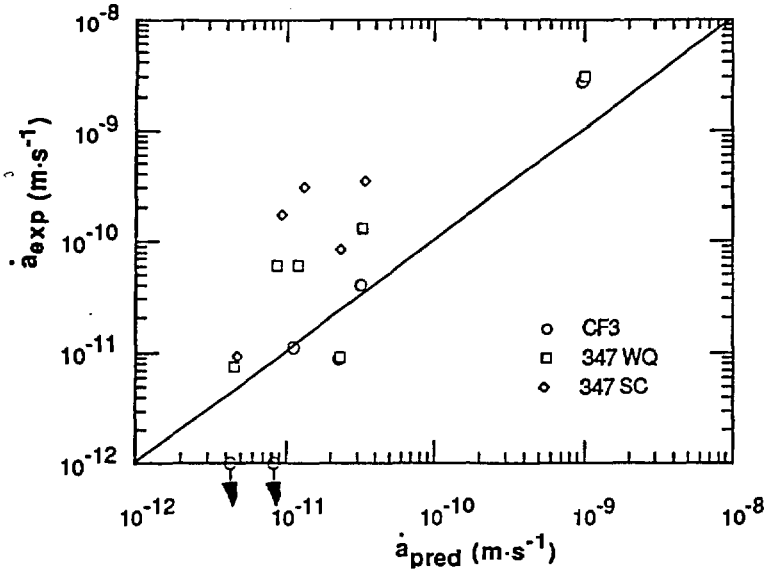

Fig. 14. Comparison of CGRs of Type 347 and CF-3 SS at 288°C in Water with 200 ppb Dissolved Oxygen and 100 ppb Sulfate with Predictions Based on ASME Section XI Reference Fatigue Crack Growth Curve in Air.

3 Conclusions

Sustained crack growth in plated and unplated specimens of a high-sulfur steel in water with 200 ppb dissolved oxygen at R = 0.95 loading was observed for stress intensity factors, K_{max}, >30 MPa·m$^{1/2}$. In most specimens, sustained crack growth under these conditions occurred only for K_{max} >40 MPa·m$^{1/2}$. This is comparable to the threshold stress intensity values for unplated specimens under R = 1 loading in water with 8 ppm dissolved oxygen.

Crack growth did not generally occur in a smooth continuous fashion. During most of the tests, crack growth rates (CGRs) were very low and were consistent with those expected under R = 0.95 loading and negligible environmental enhancement. However, rapid transient growth occurred periodically, giving rise to average crack growth rates >1 x 10^{-10} m·s^{-1}.

CGR data obtained on plated specimens at R values ranging from 0.25 to 0.9 are in reasonable agreement with the proposed ASME Section XI fatigue crack growth curves for low-alloy steels. Local slow crack growth observed under R = 0.95 loading is also in reasonable agreement with the predictions, but the transient growth and overall average CGRs greatly exceed the predictions. The magnitude of the environmental enhancement is relatively

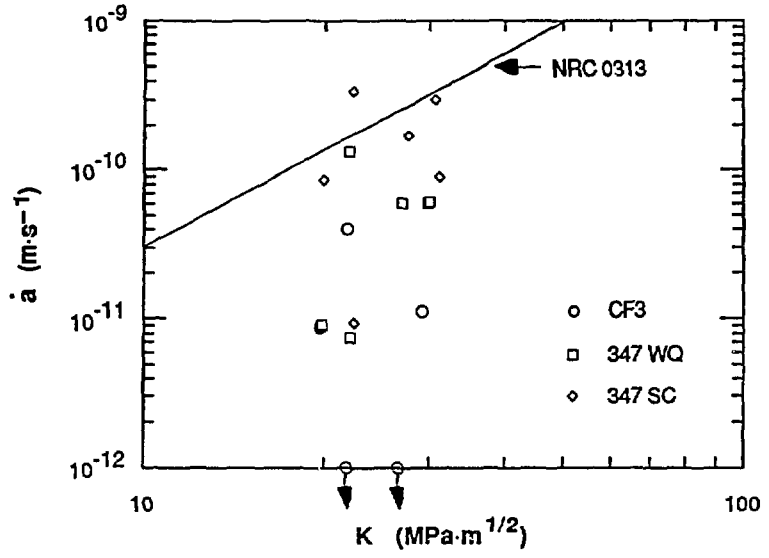

Fig. 15. Comparison of CGRs of Types 347 and CF-3 SS at 288°C in Water with 200 ppb Dissolved Oxygen and 100 ppb Sulfate with NRC Curve for Crack Growth in BWR Environments under R = 1 Loading.

consistent with that predicted, but the enhancement occurs at much lower threshold stress intensity levels than predicted.

Fatigue life of Type 316NG SS is degraded in oxygenated water for strain ranges <0.25%. Only at very low strain rates do data fall below the design curve, but there is a significant reduction in the intended margin for lives between 10^4 and 10^6 cycles. A more modest reduction in life in this range is also observed in air at 288°C.

Crack growth tests confirm the resistance of low-carbon, high-ferrite cast stainless steels to environmentally enhanced crack growth in oxygenated water.

Crack growth tests on modified Type 347 SS resulted in CGRs comparable to those observed in Type 316NG SS. The tests confirmed that the susceptibility of modified Type 347 SS to environmentally enhanced cracking is affected by heat treatment. Heat treatment seems to affect susceptibility not through sensitization, but rather through its effects on mechanical properties.

References

1. *Proc. of the Int. Atomic Energy Agency Specialists' Meeting on Subcritical Crack Growth*, NUREG/CP-0044, MEA-2014, Vols. 1 & 2 (May 1983).

2. *Proc. of the 2nd Int. Atomic Energy Agency Specialists' Meeting on Subcritical Crack Growth*, NUREG/CP-0067, MEA-2090, Vols. 1 & 2 (April 1986).

3. *Proc. of the 3rd Int. Atomic Energy Agency Specialists' Meeting on Subcritical Crack Growth*, NUREG/CP-0112, Vols. 1 & 2 (August 1990).

4. T. A. Prater, W. R. Catlin, and L. F. Coffin, *Surface Crack Growth Behavior of Structural Metals in High Temperature Water Environments*, J. Eng. Mats. and Tech. *108*, 2-9 (1986).

5. M. O. Speidel and R. M. Magdowski, *Stress Corrosion Cracking of Nuclear Reactor Pressure Vessel Steel in Water: Crack Initiation versus Crack Growth*, Corrosion 88, Paper No. 283, St. Louis, Mo, (March 1988).

6. D. A. Hale, *The Effect of BWR Startup Environments on Crack Growth in Structural Alloys*, J. Eng. Mats. and Tech. *108*, pp. 44–49 (1986).

7. F. P. Ford and P. L. Andresen, *Stress Corrosion Cracking of Low-Alloy Pressure Vessel Steels in 288°C Water*, Proc. 3rd Int. Atomic Energy Agency Specialists' Meeting on Subcritical Crack Growth, NUREG/CP-0112, Vol. 1, pp. 37–56 (August 1990).

8. P. M. Scott and D. R. Tice, *Stress Corrosion in Low Alloy Steels*, Nucl. Eng. Des. *119*, 399-413 (1990).

9. W. H. Cullen, *The Effects of Sulfur Chemistry and Load Ratio on Fatigue Crack Growth Rates in LWR Environments*, in Proc. of the 2nd Int. Atomic Energy Agency Specialists' Meeting on Subcritical Crack Growth, NUREG/CP-0067, MEA-2090, Vol. 1, pp. 339–355 (April 1986).

10. J. D. Atkinson, J. H. Bulloch, and J. E. Forrest, *A Fractographic Study of Fatigue Cracks Produced in A533B Pressure vessel Steel Exposed to Simulated PWR Primary Water Environments*, in Proc. 2nd Int. Atomic Energy Agency Specialists' Meeting on Subcritical Crack Growth, NUREG/CP-0067, MEA-2090, Vol. 2, pp. 269–290 (April 1986).

11. C. Amzallag, J. L. Bernard, and G. Slama, *French Studies of Cyclic Crack Growth Behavior of RPV Steels in PWR Environment*, in Proc. 2nd Int. Atomic Energy Agency Specialists' Meeting on Subcritical Crack Growth, NUREG/CP-0067, MEA-2090, Vol. 1, pp. 283–308 (April 1986).

12. T. Kondo, J. Kuniya, H. Takaku, K. Tokimasa, M. Arii, and M. Kurihara, *Recent Studies on Cyclic Crack Growth of Reactor Pressure Boundary Materials in High Temperature Water Environments in Japan*, in Proc. 2nd Int. Atomic Energy Agency Specialists' Meeting on Subcritical Crack Growth, NUREG/CP-0067, MEA-2090, Vol. 1, pp. 219-249 (April 1986).

13. K. Rahka, H. Hanninen, T. Saario, K. Torronen, and R. Ahlstrand, *Fatigue Crack Propagation Through Welded Cladding into Base Metal in LWR-Pressure Vessel Materials*, in Proc. 3rd Int. Atomic Energy Agency Specialists' Meeting on Subcritical Crack Growth, NUREG/CP-0112, Vol. 1, pp. 253-262 (August 1990).

14. J. Y. Park, in *Environmentally Assisted Cracking in Light Water Reactors: Semiannual Report, April 1988-September 1988*, NUREG/CR-4667 Vol. 7, ANL-89-40, pp. 38-41 (March 1990).

15. W. A. Van Der Sluys and D. S. DeMiglio, *An Investigation of Fatigue Crack Growth in SA508-2 in a 288°C PWR Environment by a Constant ΔK Test Method*, in Proc. Int. Atomic Energy Agency Specialists' Meeting on Subcritical Crack Growth, NUREG/CP-0044, MEA-2014, Vol. 1, pp. 41-64 (May 1983).

16. J. H. Bulloch, *A Review of the Fatigue Crack Extension Behaviour of Ferritic Pressure Vessel Materials in Pressurized Water Reactor Environments*, Res. Mechanica *26*, 95-172 (1989).

17. J. F. Knott, *Fundamentals of Fracture Mechanics*, John Wiley & Sons, New York (1973).

18. B. Tomkins et al., *International Cooperative Group on Cyclic Crack Growth: Tenth Anniversary Report*, Int. J. Pressure Vessels and Piping *40*, 375 (1989).

19. P. M. Scott, *A Review of Environmental Effects on Pressure Vessel Integrity*, in Proc. 3rd Intl. Symp. on Environmental Degradation of Materials in Nuclear Power Systems—Water Reactors, ed. G. J. Theus and J. R. Weeks, Metallurgical Society of AIME, Warrendale, PA (1988).

20. T. Shoji, *Quantitative Prediction of Environmentally Assisted Cracking Based on Crack Tip Strain Rate*, in Predictive Capabilities In Environmentally Assisted Cracking, PVP-Vol. 99, ed. R. Rungta, The American Society for Mechanical Engineers, New York (1985).

21. J. D. Atkinson, J. E. Forest, and D. R. Tice, *The Use of Time Based Crack Growth Data in Corrosion Fatigue Assessments*, in Proc. 2nd Int. Atomic Energy Agency Specialists' Meeting on Subcritical Crack Growth, NUREG/CP-0067, MEA-2090, Vol. 2, pp. 347-363 (April 1986).

22. G. Gabetta and K. Torronen, *Prediction of Cyclic Crack Growth Rate in LWR Environments*, in Proc. 2nd Int. Atomic Energy Agency Specialists' Meeting on

Subcritical Crack Growth, NUREG/CP-0067, MEA-2090, Vol. 2, pp. 131–152 (April 1986).

23. E. D. Eason, E. E. Nelson, and J. D. Gilman, *Reactor Pressure Vessel Steel Fatigue Crack Growth Rates in Air and Water Environments*, in Proc. of the 3rd Int. Atomic Energy Agency Specialists' Meeting on Subcritical Crack Growth, NUREG/CP-0112, Vol. 1, pp. 299–306 (August 1990).

24. E. D. Eason, S. P. Andrew, S. B. Warmbroot, E. E. Nelson, and J. D. Gilman, *Analysis of Pressure Vessel Steel Fatigue Tests in Air*, Nucl. Eng. Des. *115*, 23–30 (1989).

25. F. P. Ford and P. L. Andresen, *Corrosion Fatigue of the A533B/A508 Pressure Vessel Steels in 288°C Water*, in Proc. 3rd Int. Atomic Energy Agency Specialists' Meeting on Subcritical Crack Growth, NUREG/CP-0112, Vol. 1, pp. 105–115 (August 1990).

26. V. N. Shah and P. E. MacDonald, *Residual Life Assessment of Major Light Water Reactor Components–Overview Vol. 1*, NUREG/CR-4731, EGG-2469, Vol. 1 (June 1987).

27. H. S. Mehta, S. Ranganath, and D. Weinstein, *Application of Environmental Fatigue Stress Rules to Carbon Steel Reactor Piping*, EPRI NP-4644M Vols. 1 and 2 (July 1986).

28. D. A. Hale, S. A. Wilson, E. Kiss, and A. J. Gianuzzi, *Low-Cycle Fatigue Evaluation of Primary Piping Materials in a BWR Environment*, GEAP-20244 (September 1977).

29. K. Iida, H. Kobayashi, and M. Higuchi, *Predictive Method of Low Cycle Fatigue Life of Carbon and Low Alloy Steels in High Temperature Water Environments*, in Proc. 2nd Int. Atomic Energy Agency Specialists' Meeting on Subcritical Crack Growth, NUREG/CP-0067, MEA-2090, Vol. 2, pp. 385–409 (April 1986).

30. W. J. Shack and W. F. Burke, in *Environmentally Assisted Cracking in Light Water Reactors: Semiannual Report April—September 1988*, NUREG/CR-4667 Vol. 7, ANL-89/40, pp 15–17 (March 1990).

31. W. J. Shack, T. F. Kassner, P. S. Maiya, J. Y. Park, and W. E. Ruther, *BWR Pipe Crack Remedies Evaluation*, Nucl. Eng. Des. *108*, 199–210 (1988).

32. S. Susuki, S. Itoh, H. Isokibe, S. Miyajuma, H. Shidawara, S. Kawashima, M. Asano, K. Enomoto, M. Higuchi, and G. Nakano, *Fatigue Strength of Austenitic Stainless Steels in Simulated BWR Environment*, Proc. of the 1987 Annual Meeting of the Atomic Energy Society of Japan, Nagoya, Japan.

33. W. E. Ruther, W. K. Soppet, J. Y. Park, and T. F. Kassner, in *Environmentally Assisted Cracking in Light Water Reactors: Semiannual Report, October 1986–March 1987*, NUREG/CR-4667 Vol. IV, ANL-87-41, pp. 1–3 (December 1987).

34. P. S. Maiya, in *Environmentally Assisted Cracking in Light Water Reactors: Semiannual Report April–September 1987*, NUREG/CR–4667 Vol. 5, ANL–88/32, pp 9–16 (March 1990).

35. W. E. Ruther, J. Y. Park, T. F. Kassner, and W. K. Soppet, in *Environmentally Assisted Cracking in Light Water Reactors: Semiannual Report, October 1988–March 1989*, NUREG/CR–4667 Vol. IV, ANL–90–4, pp. 2–5 (June 1990).

36. N. R. Hughes, W. L. Clarke, and D. E. Delwiche, *Intergranular Stress-Corrosion Cracking Resistance of Austenitic Stainless Steel Castings, Stainless Steel Castings*, ASTM STP 756, eds. V. G. Behal and A. S. Melilli, American Society for Testing and Materials, pp. 26–47 (1982)

37. W. S. Hazelton, *Technical Report on Material Selection and Processing Guidelines for BWR Coolant Pressure Boundary Piping*, NUREG–0313, Rev. 2 (June 1986).

Acknowledgments

W. F. Burke, D. R. Perkins, W. K. Soppet, G. J. Talaber, and J. C. Tezak contributed to the experimental effort in this program.